Mesoscale Variability and Drizzle in Southeast Pacific Stratocumulus

KIMBERLY K. COMSTOCK, CHRISTOPHER S. BRETHERTON, AND SANDRA E. YUTER

University of Washington, Seattle, Washington

(Manuscript received 12 November 2004, in final form 24 March 2005)

ABSTRACT

Observations from the East Pacific Investigation of Climate (EPIC) 2001 field campaign are well suited for exploring the relationships among the diurnal cycle, mesoscale (10–100 km) structure, and precipitation in the stratocumulus region in the southeast Pacific. Meteorological time series and observations from a scanning C-band radar, vertically pointing cloud radar, and ceilometer, as well as satellite data, are used to show that drizzle is associated with increased variability in cloud and boundary layer properties compared to nondrizzling periods. The stratocumulus-topped boundary layer is typically well mixed at night, transitioning to less well mixed in the afternoon, with drizzle most frequently occurring in the early morning. Coherent patches of drizzle, or "cells," can have large areas with radar reflectivities of greater than 5 dBZ of up to about 100 km^2. Individual cells have long lifetimes, up to 2 h, and appear to be replenished by moisture in the boundary layer.

1. Introduction

In the subtropics, large regions of stratocumulus (Sc) clouds lie trapped between warm subsiding air and the cool sea surface off the west coasts of continents. These Sc clouds are relatively warm, with tops less than 1–2 km, so they emit nearly as much longwave radiation as the sea surface beneath them. The Sc clouds are also typically optically thick, reflecting much of the incident solar radiation. Because of these characteristics and the vast areal extent of the Sc regions, these clouds have a significant cooling effect on the earth's radiation budget (Hartmann et al. 1992). The radiative properties of Sc are dependent on cloud thickness and cloud fraction. These, in turn, are regulated by small-scale turbulent fluxes and a complex set of interactions within the shallow marine boundary layer. Currently, most climate models poorly represent the Sc cloud properties relevant to albedo (e.g., Delecluse et al. 1998).

Even if we could perfectly parameterize the properties of a horizontally homogeneous Sc layer in a grid column of a climate model, there is another complication, which is a principal motivation for our study. Satellite images of subtropical Sc usually show distinct "mesoscale" modulation of cloud properties. [Here, we take mesoscale to be 10–100-km wavelength, which is "mesobeta" scale according to Orlanski (1975).] This mesoscale horizontal variability of cloud properties affects the radiative properties of the Sc region (e.g., Wood and Hartmann 2004; Rossow et al. 2002).

Horizontally homogeneous unbroken Sc clouds are interspersed with mesoscale regions of broken cloud consisting of open- or closed-cell cellular convection. Closed cells are patterns of cloudy regions surrounded by clear air; these cells typically occur over cool water near coasts (e.g., Agee et al. 1973). Open cells are clear regions surrounded by "rings" of clouds that occur most commonly in outbreaks of cold air over warmer water (e.g., Atkinson and Zhang 1996), where convection is primarily driven by surface fluxes rather than the cloud-top radiative cooling that is the main turbulent mixing mechanism in closed-cell convection (Agee and Lomax 1978; Brümmer et al. 1986). Oceanic trade cumuli also frequently organize into open cells. Regions of open and closed cells can coexist and can evolve into each other, and linear cloud features called actinae are sometimes observed in transitional regions (Garay et al. 2004).

Stratocumulus clouds exhibit a strong diurnal cycle, which was first documented by Kraus (1963) in the northeast Pacific. Later, the diurnal cycle of Sc was

Corresponding author address: Kimberly K. Comstock, Dept. of Atmospheric Sciences, University of Washington, Box 351640, Seattle, WA 98195.
E-mail: kcomstock@atmos.washington.edu

more comprehensively analyzed using aircraft observations in the North Sea (Nicholls and Turton 1986) and during the 1987 First International Satellite Cloud Climatology Project (ISCCP) Regional Experiment (FIRE) off the coast of southern California (Cox et al. 1987). At night, the boundary layer tends to be well mixed (or coupled). Strong longwave cooling drives mixing throughout the boundary layer as negatively buoyant air parcels at the top of the cloud sink toward the surface, also driving more cloud-top entrainment. After the sun rises, shortwave absorption in the cloud layer decreases the cloud-top cooling effect. This leads to less energetic mixing during the day, especially below cloud base. The boundary layer can become decoupled if mixing no longer extends through the cloud and surface layers. After the sun sets, the cycle repeats as cloud-top longwave cooling rejuvenates mixing in the boundary layer.

Stratocumulus clouds tend to thicken during the night. Consequently, the formation of drizzle by coalescence becomes more likely as morning approaches. Drizzle is important to the boundary layer dynamics and therefore the cloud properties. The evaporation of drizzle can help to stabilize the boundary layer by cooling the subcloud region. As part of FIRE, Paluch and Lenschow (1991) observed mesoscale regions beneath precipitating Sc clouds where the evaporation of drizzle cooled and moistened the subcloud layer. Large-eddy simulations of nocturnal Sc clouds indicate that this evaporation of drizzle can inhibit heat and moisture flux just below the cloud, leading to favorable conditions for more patchy cloud conditions (Stevens et al. 1998). Strong drizzle events were observed in patchy cloud conditions during the Atlantic Stratocumulus Transition Experiment (ASTEX) in the northeast Atlantic (Austin et al. 1995). During the second Dynamics and Chemistry of Marine Stratocumulus experiment (DYCOMS II; Stevens et al. 2003) off the coast of California, patchy, open-cell structures within the closed-cell Sc clouds were associated with enhanced precipitation compared to closed cells (Stevens et al. 2005). Sharon et al. (2004, manuscript submitted to *J. Atmos. Sci.*) found similar results in the northeast Pacific.

In this study, we use several comprehensive datasets to characterize open- and closed-cell Sc clouds, as well as the role of drizzle and the diurnal cycle. We also show that drizzle is associated with increased variability of state parameters within mesoscale regions of broken cloud. Mesoscale regions of broken cloud have reduced area-mean albedo compared to the same amount of liquid water in an unbroken Sc cloud region. We use shipboard, buoy, and satellite data from the East Pacific Investigation of Climate (EPIC) 2001 Sc field campaign (Bretherton et al. 2004), which provided the most comprehensive observational dataset to date of southeast tropical Pacific Sc clouds. This region has the additional advantage of long-term monitoring of radiative fluxes and surface meteorological variables by a Woods Hole Oceanographic Institution (WHOI) Improved Meteorological (IMET) buoy, stationed at 20°S, 85°W since October 2000 (Cronin et al. 2002).

The datasets used in this study are described in section 2. Subsequent sections describe the analysis of the time series data using Fourier and cross-spectral analysis and the classification and characterization of drizzling, coupled, and less-coupled regimes. Individual drizzling cells are tracked to characterize their life cycle. The material from the previous sections is distilled into a conceptual model and summarized in the final two sections.

2. Data

This analysis synthesizes several sets of observations available for the austral spring at 20°S, 85°W, including data collected on the National Oceanic and Atmospheric Administration (NOAA) Research Vessel *Ronald H. Brown* (*RHB*), an IMET buoy, and by geostationary satellites. The *RHB* was equipped with instrumentation measuring surface meteorology, and turbulent and radiative fluxes, as well as a laser ceilometer, two meteorological radars, and rawinsondes. Data from shipboard instruments used in this analysis are from the 6 days that the *RHB* spent at the buoy location during EPIC 2001 Sc, 16–21 October 2001 [the "on-station period," which Bretherton et al. (2004) called the buoy period].

The set of shipboard meteorological time series, obtained from the NOAA/Environmental Technology Laboratory (ETL) instrumentation, includes downwelling longwave and solar radiation (LW and SW), wind speed (U) and direction, temperature (T), pressure, and relative humidity (RH), all measured at 15 m above sea level and averaged over 5-min intervals. The latter three series were used to calculate water vapor mixing ratio (q) and lifting condensation level (LCL) as in Bolton (1980). Time series of potential temperature (θ) and virtual temperature (T_v) were also computed.

An ETL laser ceilometer provided cloud-base heights at 15-s intervals. To reduce contamination by sporadic ceilometer returns off drizzle below cloud base, we derived lower-frequency cloud-base data series by computing the median of the 15-s measurements over specified time intervals.

The ETL vertically pointing 8.6-mm-wavelength

cloud radar (MMCR) had a 0.5° beamwidth and obtained a profile every 10 s during EPIC 2001 Sc. The vertical resolution of the MMCR was 90 m, and its dynamic range was from approximately −45 to 20 dBZ at a height of 1.3 km (Moran et al. 1998). Both saturation and minimum detectable reflectivity values decrease closer to the radar. In heavy drizzle, the MMCR occasionally saturated below or even in the cloud (Comstock et al. 2004). The MMCR was calibrated to within about 1 dBZ (D. Hazen 2002, personal communication). MMCR reflectivity profiles were used to determine cloud-top heights. Linear interpolation was performed on the cloud-base and cloud-top time series over short periods where data were unavailable.

EPIC 2001 Sc was only the second field project, after the 1997 Pan American Climate Studies Tropical Eastern Pacific Process Study (TEPPS Sc; Yuter et al. 2000), to use a scanning C-band radar to explore the structure of drizzle in Sc clouds. With one complete 30-km-radius volume collected every 5 min, this dataset is particularly well suited to analyzing both the structure and the evolution of drizzle cells. The 5-cm-wavelength C-band radar is sensitive to drizzle and heavier precipitation but not clouds (Ryan et al. 2002). The minimum reflectivity detectable by the radar was about −12 dBZ at 30 km. The C-band calibration uncertainty was estimated as ±2.5 dBZ by Comstock et al. (2004). The scan strategy for the C-band radar and the interpolation procedure applied to the data are presented in appendix A of Comstock et al. (2004). To circumvent errors in the vertical position of individual returns caused by radar pointing-angle uncertainties during volume scans, a 2D C-band radar reflectivity dataset was created by vertically averaging the 3D data between 0.5 and 2 km (Comstock et al. 2004). This captured the mean cloud layer, which was between 900 and 1200 m. The C-band radar data were interpolated to a horizontal resolution (pixel size) of 500 m by 500 m. Despite the strong inversion observed in the EPIC 2001 Sc region, the C-band radar was not found to be sensitive to Bragg scattering.

Vaisala RS-80 rawinsondes were released from the *RHB* 8 times a day throughout the EPIC 2001 Sc cruise. Three-hourly profiles of RH, q, and θ were derived from quality controlled upper-air sounding data (Bretherton et al. 2004).

The WHOI IMET buoy has been moored at 20°S, 85°W, since October 2000 (Cronin et al. 2002). Three year-long time series through November 2003 were obtained (courtesy of Dr. R. A. Weller). The dataset includes time series of LW and SW radiation, T, q, U, and T_v (computed as for the ship series). All data were provide once per minute and were averaged to 2-min values to reduce noise.

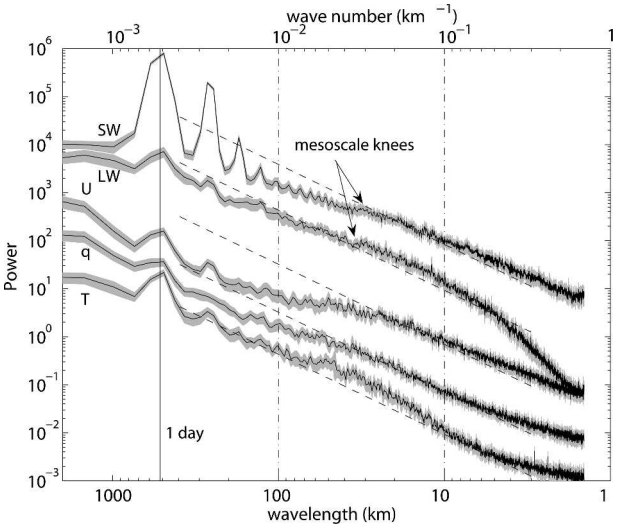

FIG. 1. Power spectra for buoy time series of surface temperature T, water vapor mixing ratio q, wind speed U, downwelling longwave radiation LW, and shortwave radiation SW scaled to fit on the same plot. The 95% confidence intervals are shaded. Dashed lines are of slope $k^{-5/3}$, where k is wavenumber (top abscissa). The distance scales (abscissas) were converted from time using an average wind speed of 6 m s^{-1}. The vertical solid line marks the diurnal peak, and the vertical dash–dot lines correspond to the mesoscales. "Mesoscale knees," or changes in spectral slope, are labeled on two of the five spectra.

Images from the Geostationary Operational Environment Satellite (GOES) are also used in this analysis (Menzel and Purdom 1994). Both GOES visible (channel 1, 0.55–0.75 μm, 1 km) and infrared (IR, channel 4, 10.2–11.2 μm, 4 km) images provide contextual information.

3. Fourier and cross-spectral analysis

Fourier spectral and cross-spectral analyses were used to determine general characteristics of the buoy meteorological time series. Power spectra for T, q, U, LW, and SW were calculated using Welch's averaged periodogram method (Welch 1967). We used buoy data only during September, October, and November (SON) for each year, because this is the season with peak Sc cloud cover (e.g., Klein and Hartmann 1993) and because these times are most comparable to the EPIC 2001 Sc cruise data. We divided each buoy data series into segments of length 4096 points (5.7 days) and applied a Hanning window to individual segments, which overlapped by 50%.

Power spectra for T, q, U, LW, and SW from the 3 yr of SON buoy data are shown in Fig. 1. At low frequen-

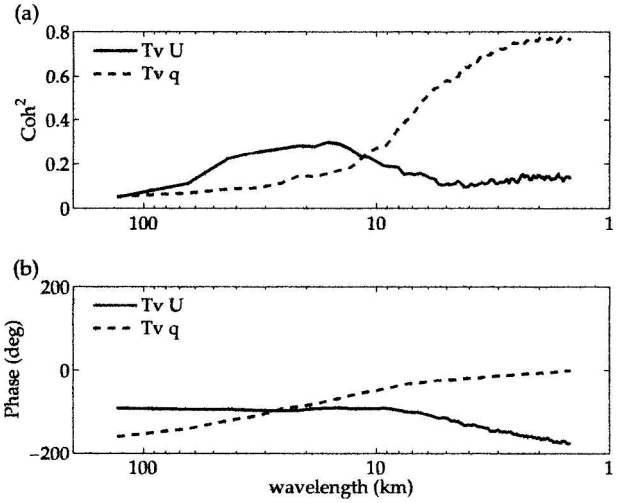

FIG. 2. Cross-spectral analysis for SON buoy time series. (a) Magnitude-squared coherence between virtual temperature T_v and wind speed U (solid), and T_v and mixing ratio q (dashed). The 99% confidence level is ~0.004. (b) Phase between T_v and U (solid) and between T_v and q (dashed). The scale on the abscissa was converted from time to distance using an average wind speed of 6 m s^{-1}.

cies, each spectrum is dominated by a distinct peak corresponding to the diurnal cycle that modulates the Sc region (Bretherton et al. 2004). At the highest frequencies, spectra of T and q are most likely flattened due to a noise floor. The smallest scales are unresolvable to the LW radiometer, causing the observed dropoff of power in the LW spectrum below ~5 km.

Studies such as Nastrom and Gage (1985) have shown that power spectra of wind speed and θ have a $k^{-5/3}$ slope, where k is the wavenumber, for wavelengths between 3 and 300–400 km in the free troposphere. Dashed lines of $k^{-5/3}$ slope shown in Fig. 1 aid in viewing the spectral break present in the 10–100-km mesoscale region for each of the spectra (even though $-5/3$ is not necessarily the expected slope for LW or SW). These features, two of which are labeled as mesoscale knees, warrant a closer look at the boundary layer processes that may be affecting the spectral slope on the mesoscales.

We focus the rest of our spectral analysis on mesoscale phenomena. To help interpret the mesoscale signals, we performed cross-spectral analysis, averaging spectra for over 1220 six-hour (~130 km) data segments during the months of September, October, and November between 2000 and 2003. Figure 2a shows computed values of magnitude-squared coherence, or the correlation (squared), between T_v and U, as well as T_v and q, at each wavelength. Using 2 degrees of freedom for each of the 1220 spectral estimates, the 99% confidence level is ~0.004 following von Storch and Zwiers (1999, p. 284). Therefore, the coherence-squared values for both T_v and U and T_v and q are statistically significant in the 10–100-km mesoscale range, although those for T_v and q are much more coherent at sub-10-km scales.

Figure 2b shows the phase of the relationships between the sets of variables at each wavelength. The phase information should be considered reliable only where the coherence of the variables is statistically significant. This figure shows that T_v and U are approximately in quadrature for scales between 10 and 100 km, with U leading T_v by about 90°. This quadrature relationship implies along-wind convergence (thus rising air) in mesoscale warm regions and corresponding divergence (sinking air) in cooler regions.

Figure 2b also shows that T_v and q are nearly 180° out of phase at 100-km wavelengths, corresponding to mesoscale pockets of warm (dry) and cool (moist) air near the surface. At smaller scales, T_v and q tend toward an in-phase relationship, consistent with warm (moist) eddy updrafts and cool (dry) eddy downdrafts that produce upward surface buoyancy and latent heat fluxes.

Although the shorter time series in the 6-day ship data are associated with more noise, results from spectral and cross-spectral analyses of ship time series (not shown) are consistent with the results shown in Figs. 1 and 2.

4. Subdividing the ship time series into three regimes

a. Mean properties

Bretherton et al. (2004) showed that the diurnal cycle of the southeast Pacific Sc-topped boundary layer generally follows the nighttime or early morning precipitation and cloud-top maximum described in the introduction. Unlike in the northeast Pacific, however, cloud base in the southeast Pacific remains fairly constant while cloud top rises at night and sinks during the day due to a pronounced diurnal cycle of subsidence (Bretherton et al. 2004) and entrainment (Caldwell et al. 2005).

To further illuminate the processes in the Sc-topped boundary layer, we find it useful to subdivide the ship observations into three regimes—drizzling, coupled (or well mixed), and less coupled—and to analyze the characteristics of each regime separately. The boundary layer was classified as drizzling when the C-band radar area of reflectivity greater than 5 dBZ was larger than 120 km^2, or about 4% of the C-band echo area, using

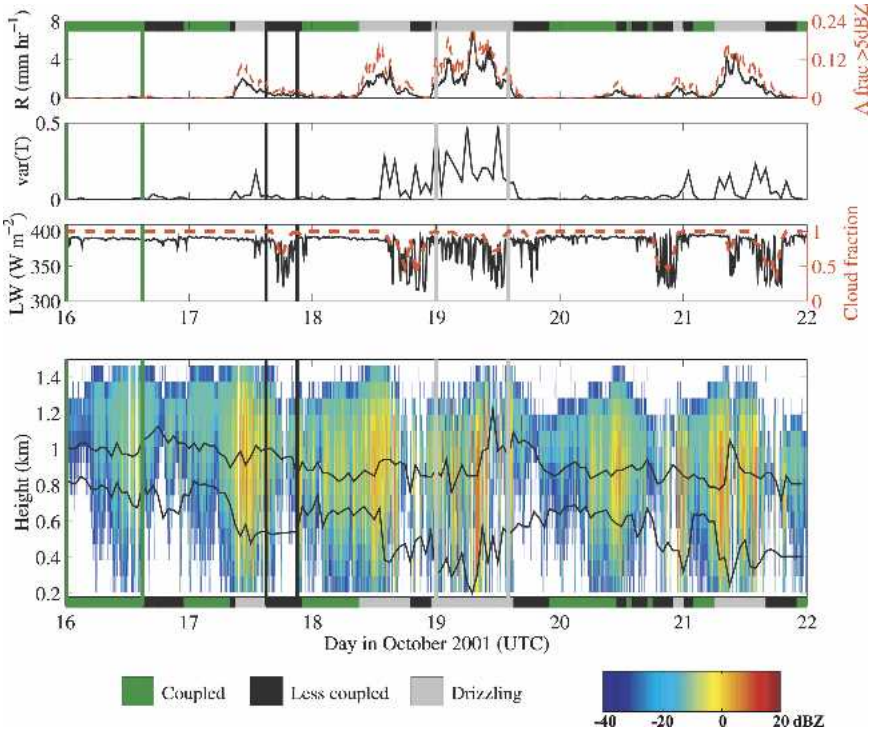

FIG. 3. On-station period time series. (top) The 5-min area-averaged rain rate R (black) and area fraction with reflectivity greater than 5 dBZ (red dashed) from the C-band radar. (second from top) Hourly bandpass-filtered variance of 5-min resolution surface air temperature, T, from the ship. (third from top) The 5-min downwelling longwave radiation LW at the ship (black) and hourly cloud fraction from the ceilometer (red dashed). (bottom) The 1-min MMCR reflectivity profiles. Hourly cloud base (CB) and LCL are plotted in black. Coupled (green), less coupled (black), and drizzling (gray) hours are depicted by bars at the top and bottom of the figure. Examples of coupled, less coupled, and drizzling time periods are highlighted with vertical lines. Local time is 6 h earlier than UTC time.

interpolated cloud reflectivity with 500 m × 500 m pixels. The 120 km^2 threshold serves as an objective way to distinguish between drizzling and nondrizzling radar volumes, and it agrees well with subjective assessments of the same data. It establishes a drizzling regime when a single large drizzle cell or several small cells enter the C-band field of view.

Time series of the area-averaged rain rate (from Comstock et al. 2004) and the corresponding C-band radar echo area fraction with reflectivity greater than 5 dBZ are shown in the top panel of Fig. 3.

The difference between hourly ceilometer-derived cloud-base height and hourly average LCL served to subdivide the nondrizzling data. When this difference was less than 300 m, the boundary layer was categorized as coupled for the entire hour; otherwise, it was classified as less coupled. The difference between observed and predicted cloud-base height is used to make this distinction because it is expected that this quantity will be relatively small for a well-mixed (coupled) boundary layer.[1] The differences are larger for a less-coupled boundary layer, where the processes at the surface and in the cloud are not as closely tied. Note that during the EPIC 2001 Sc on-station period, the boundary layer never exhibited manifestations of pronounced decoupling, such as a distinct layer of "scud" or cumulus below the stratocumulus cloud base, or a strong upward decrease in humidity exceeding 1–2 g kg^{-1} over the boundary layer depth.

[1] The distance between the calculated LCL and cloud base would be greater than zero even in a well-mixed boundary layer because the LCL is calculated from measurements obtained in the surface layer. For the mean air–sea temperature and humidity differences observed in EPIC 2001 Sc, and using a log-layer model of the surface layer, the LCL calculated from ship measurements would be 150 m lower than the LCL of air at 130 m, which roughly corresponds to a nominal top of the surface layer at 10% of the boundary layer height.

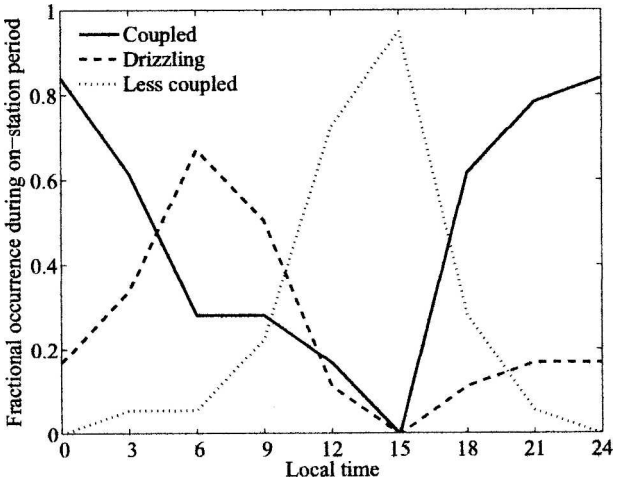

FIG. 4. Probability density functions showing composite 6-day diurnal cycle of coupled, drizzling, and less-coupled hours during the on-station period.

The classification (coupled, less coupled, or drizzling) for each hour during the on-station period is shown in the top and bottom panels of Fig. 3. In addition, one several-hour example of each regime is highlighted with vertical lines through each panel in Fig. 3. Hourly cloud-base and LCL time series, overlaid onto the time–height section of MMCR reflectivity, show that the calculated LCL and cloud base track closely during coupled time periods but are much farther apart during less-coupled periods. When there was drizzle directly over the ship, the ceilometer sometimes provided an anomalously low cloud base, perhaps detecting below-cloud drizzle instead of cloud. Even after we accounted for this, the cloud base–LCL differences were still largest when drizzle occurred in the area.

Figure 4 shows the mean diurnal cycle of the frequency of drizzling, coupled, and less-coupled hours during the on-station period. Compositing the hours classified in each regime during the on-station period, we find, as expected, that the coupled regime dominates early in the night, the less-coupled regime in the afternoon, and drizzle occurs most often in the early morning.

Mean properties for each boundary layer regime are summarized in Table 1. Cloud base was lowest for the drizzling regime, but the mean cloud thickness during the drizzling regime (including breaks with zero cloud thickness) was just slightly greater than during the coupled regime. Clouds were thinner during the less-coupled regime, mostly due to a lower cloud top. Mean surface moisture was greater for the drizzling and less-coupled regimes than for the coupled regime. At night, enhanced entrainment (Caldwell et al. 2005) may have aided in drying the coupled boundary layer. In the afternoon, the mixing of moist air away from the surface is likely to be less effective during the less-coupled regime. The evaporation of drizzle assumably moistened the surface air in the drizzling regime.

These features are illustrated in Fig. 5, which shows mean profiles of RH for each regime. Individual profiles used to compute the mean are from rawinsonde soundings during the on-station period and have been normalized by the height of the subsidence inversion. The mean coupled profile is that of a typical mixed layer, with RH increasing to saturation at the cloud base. The cloud fraction was 1.0 during the coupled regime (Table 1), indicating unbroken clouds. In comparison, the less-coupled profile is relatively more moist near the surface and relatively drier just below and in the cloud layer. The mean less-coupled profile does not reach saturation in the "cloud layer" because in five of the seven constituent profiles the rawinsonde ascended through a break in the clouds. Table 1 indicates that the less-coupled regime was associated with the lowest cloud fraction (0.87). The drizzling regime was also not completely overcast; in fact, 2 of the 16 rawinsonde ascents during the drizzling regime occurred in cloud breaks. The mean drizzling profile has higher RH at all heights below cloud base than the other regimes.

Figure 6 shows all 48 soundings of θ and q, normalized by the inversion height and categorized according to the state of the boundary layer when the rawinsonde was launched, as well as mean soundings for the three regimes. The individual profiles show some variability,

TABLE 1. Mean properties of the ship data in coupled, less-coupled, and drizzling boundary layer (BL) regimes. The time column records the percent of on-station period hours categorized in each regime; q is the mixing ratio; cloud base (cb), top (ctop), thickness (cthk), and fraction (CF) are all averaged for hourly values. LCL is the lifting condensation level, SST $-$ T is the mean air–sea temperature difference, and $A > 5$ dBZ is the percent of the C-band echo area with reflectivity greater than 5 dBZ during each regime.

BL regime	Time (%)	q (g kg^{-1})	cb (m)	ctop (m)	cthk (m)	CF (m)	LCL	T − SST (K)	$A > 5$ dBZ (%)
Coupled	45	8.6	926	1257	331	1.00	704	−1.3	0.5
Less coupled	29	9.3	932	1161	229	0.87	527	−1.6	1.5
Drizzling	26	9.3	916	1263	347	0.93	445	−2.2	10.0

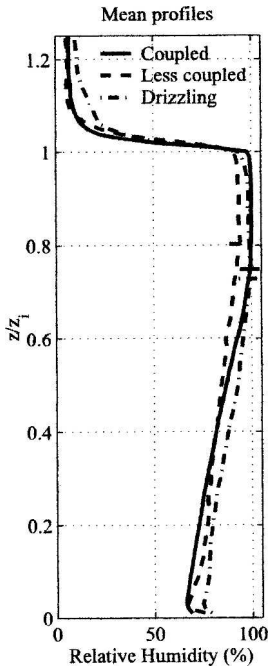

FIG. 5. EPIC 2001 Sc on-station period mean soundings of relative humidity, normalized with respect to the inversion height, z_i, for each regime: coupled (solid), less coupled (dashed), and drizzling (dash–dot). Mean cloud-base heights for each regime are marked with horizontal lines in corresponding line types.

but in general illustrate the considerable degree to which the southeast Pacific boundary layer was well mixed during the EPIC 2001 Sc 6-day on-station period. All of the coupled soundings are quite well mixed, while some drizzling soundings are relatively well mixed and others are less so. Neither less-coupled nor drizzling soundings show a preferred level at which vertical gradients are concentrated. Again, the mean drizzling profile is cooler and more moist than the others due to below-cloud evaporation of precipitation.

b. Variability

Mesoscale bandpass-filtered time series are useful for examining mesoscale temperature and moisture covariability in each of the boundary layer regimes. To isolate mesoscale variability in the ship on-station period meteorological datasets, time series were bandpass filtered using a sixth-order Butterworth digital filter, with half-power at 30 min and 6 h. Given a typical boundary layer wind speed of 6 m s^{-1}, this corresponds to wavelengths roughly between 10 and 100 km.

Paluch and Lenschow (1991) examined low-pass-filtered aircraft data (roughly equivalent to our bandpass-filtered data) taken during the field project FIRE in Sc off the coast of California. They found that the slope of the scatterplot of θ versus q fell along a pseudoadiabat and interpreted this as a signature of evaporation of patchy drizzle within the subcloud layer. Figure 7 shows an analogous analysis for our data. Scatterplots of bandpass-filtered T versus q are shown for unsegregated data as well as data segregated into coupled, less coupled, and drizzling regimes. The lines correspond to constant moist static energy, h (a pseudoadiabat), and constant virtual temperature, T_v. Points falling along the latter line indicate a buoyancy-compensated situation where there are warmer, drier patches and cooler, moister patches of nearly the same T_v.

The scatterplot in Fig. 7a shows all data for the on-station period. More physical insight is gained by subdividing the data into the three regimes. For the coupled regime (Fig. 7b), the data mostly cluster along a line of constant T_v. However, looking closely, we find that the slope of the data is roughly zero (the 99% confidence limits on the slope are -0.07 and 0.03, with a standard error of the regression of about 0.1). The zero slope suggests that moister parcels tend to be somewhat warmer than they would be if T_v were constant and, conversely, drier parcels tend to be cooler. This implies a direct mesoscale circulation as warm, moist, more-buoyant parcels rise, and cooler, drier, less-buoyant parcels sink. This finding corroborates evidence for such circulations shown in Fig. 2.

For the less-coupled regime (Fig. 7c), most of the points fall along the constant T_v line, though with greater scatter than in the coupled regime. The drizzling regime (Fig. 7d) shows even greater variance. We find some evidence of mesoscale effects of evaporative cooling, as points tend to lie closer to the line of constant h than in the other regimes, though it is not as pronounced as in the Paluch and Lenschow study. Other studies have also found evidence of evaporation of drizzle in cooler and more moist air beneath precipitating clouds (e.g., Austin et al. 1995; Wood 2004).

In addition to temperature and moisture, the drizzling regime is also associated with the highest variance of other cloud and boundary layer properties. Table 2 provides standard deviations for the 5-min bandpass-filtered data for each boundary layer regime. The coupled regime has the lowest mesoscale variance (is the most horizontally homogeneous). The drizzling regime, on the other hand, has the largest standard deviation for all quantities, with particularly large enhancements in T (0.42 versus 0.10 K) and cloud thickness (151 versus 60 m) compared to the coupled regime. The less-coupled regime shows enhanced variability

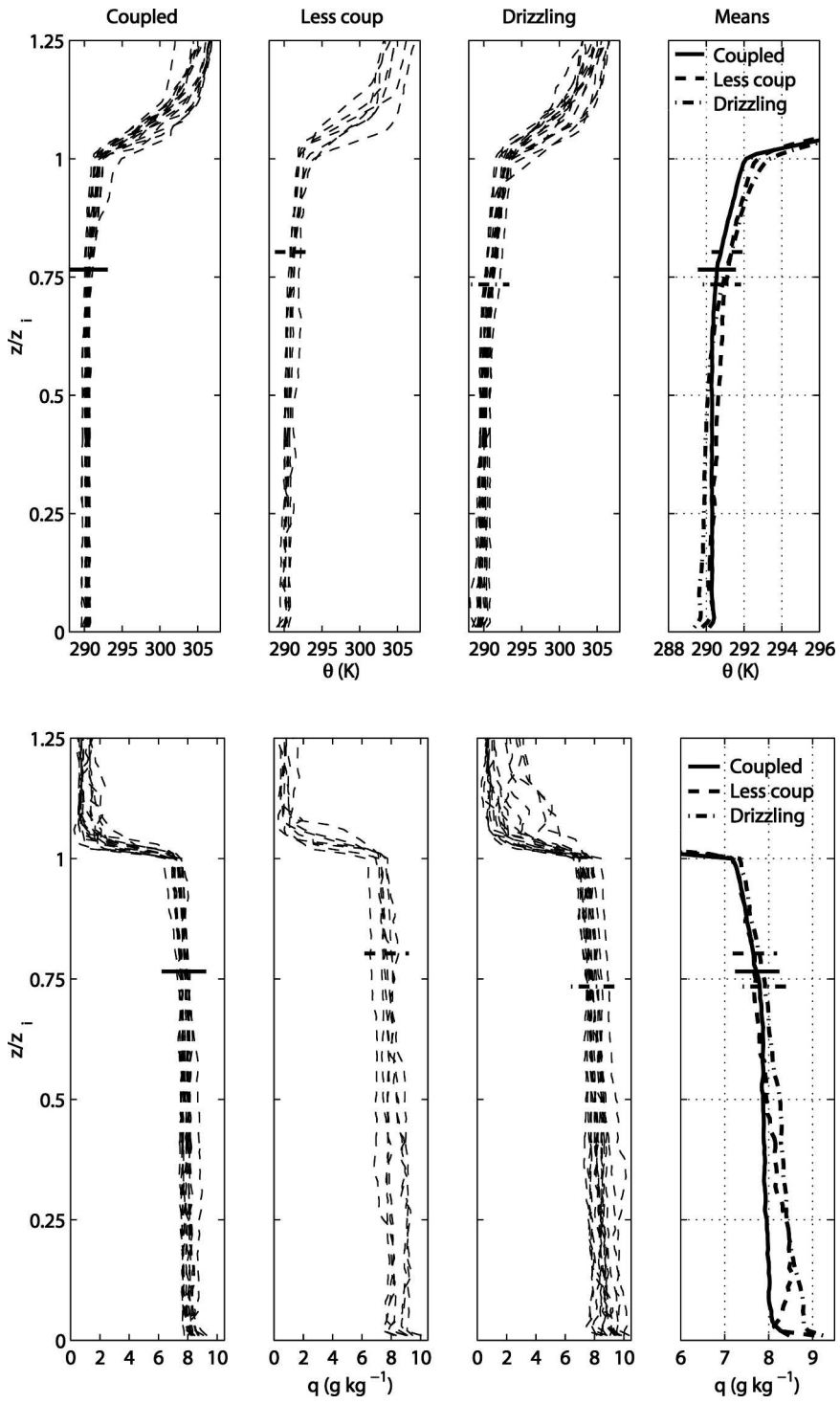

FIG. 6. EPIC 2001 Sc on-station period soundings of q and θ, normalized with respect to the inversion height, z_i. The left three sets of panels show individual sounding profiles during the on-station period, divided by regime. The far-right panels show composite profiles for each regime: coupled (solid), less coupled (dashed), and drizzling (dash–dot). Mean cloud-base heights are marked with horizontal lines in each panel in corresponding line types for each regime. The scales on the abscissas differ for the mean profiles.

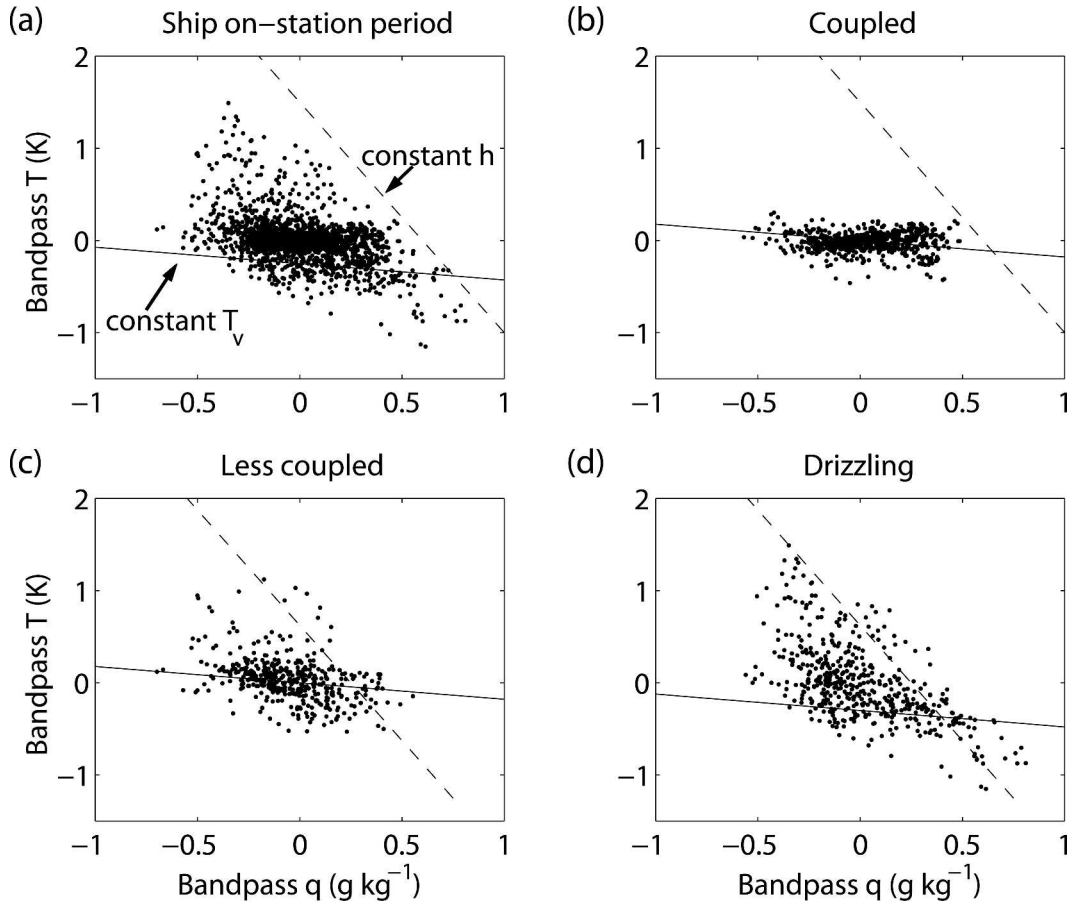

FIG. 7. Bandpass-filtered temperature T vs bandpass-filtered water vapor mixing ratio q for (a) the entire 6-day on-station period, (b) the coupled regime, (c) the less coupled regime, and (d) the drizzling regime. Lines of constant moist static energy h (dashed) and virtual temperature T_v (solid) are also drawn in each subplot.

compared to the coupled regime [also found by other studies; e.g., Moyer and Young (1994)], but less than during drizzle.

Figure 3 illustrates the increased variance of boundary layer and cloud properties associated with the drizzling regime. The periods of high area-averaged rain rate, shown in the top panel, correspond with episodes of high hourly variance of the surface temperature T (second panel) driven by the evaporation of patchy drizzle. Most of these episodes also coincide with periods of high variance in the cloud thickness and broken clouds, as indicated in the third panel by episodes of decreased downwelling LW and lower cloud fraction. In section 6 we will further explore the correlations between measured variables in individual regimes.

5. Characterization of drizzle cells

The time–height profile of radar reflectivity in Fig. 3 indicates short-lived periods of high reflectivity (drizzle) passing over the ship. These can be seen more clearly with the C-band radar. An example from 0905

TABLE 2. Standard deviations for mesoscale bandpass-filtered ship data series in coupled, less-coupled, and drizzling regimes. Columns are for temperature, water vapor mixing ratio, wind speed, cloud base, cloud top, cloud thickness, and cloud fraction.

Parameter	T (°C)	q (g kg^{-1})	U (m s^{-1})	cb (m)	ctop (m)	cthk (m)	CF
Coupled	0.10	0.20	0.65	34	38	60	0.03
Less coupled	0.24	0.21	0.80	68	83	111	0.15
Drizzling	0.42	0.26	1.04	117	95	151	0.15

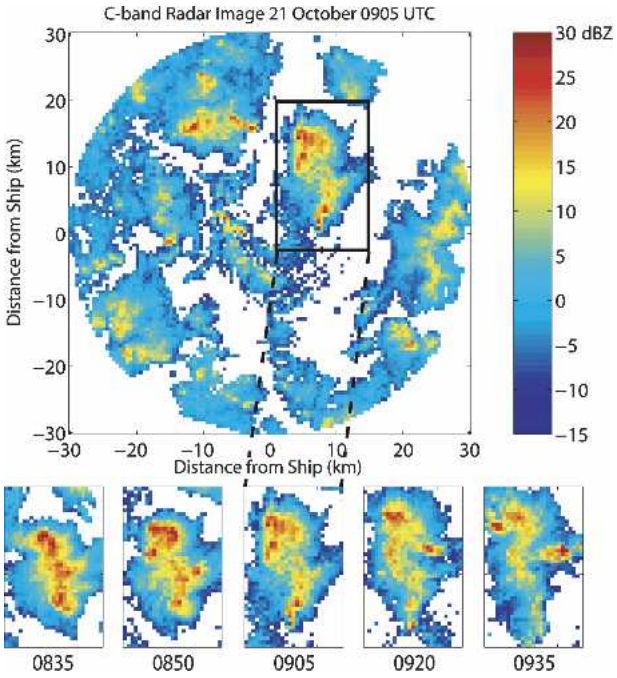

FIG. 8. The C-band radar image from 0905 UTC 21 Oct 2001, and small "cutout" images of a cell every 15 min as it evolved with time.

UTC on 21 October is shown in the top panel of Fig. 8. Throughout the on-station period, the C-band radar detected a large number of these drizzling regions ("cells") that appeared to advect with the mean wind. We defined drizzle cells as contiguous regions with reflectivity greater than 5 dBZ. The larger and more cohesive cells lasted upward of 1.5–2.0 h before being advected out of the radar's range. The cells ranged in size from just detectable up to about 100 km^2. Drizzle cells are the precipitating portions of Sc clouds, and mesoscale cellular patterns of cloud organization are at times present in the reflectivity maps. The results of section 4 suggest drizzle may enhance mesoscale variability, motivating a careful look at the life cycle of drizzle cells.

We chose eight drizzle cells to follow closely. For ease of the analyses, particularly identification from one image to the next, we selected only large cells with relatively high reflectivity. Table 3 summarizes the characteristics of each of the cells. We constructed bounding boxes of appropriate sizes to encompass each cell throughout its observed lifetime in the C-band data. The size of each cell's bounding box (Table 3) remained constant in time. Each box was "advected" with the cell advection speed, which was calculated roughly by maximizing the spatial lag correlation of radar reflectivity exceeding 0 dBZ between successive C-band images. Computed advection direction and speeds matched reasonably well with surface wind velocities and rawinsonde-sampled boundary layer winds.

Figure 8 shows a C-band radar reflectivity image of cell 6 (see Table 3) with its bounding box. The lower panels of the figure depict the cell's evolution every 15 min during 1 h of its observed lifetime. During this time, the cell appears to split, spread, and then dissipate.

The average reflectivity with time was calculated for each of the eight example cells. Average reflectivities were computed within each bounding box, not including missing data or reflectivity values below the C-band minimum detectable limit of −12 dBZ; both shown as white space in Fig. 8. Although the entire life cycle was not captured for any single drizzle cell, individual cells represent different portions of a typical life cycle because some were growing while others dissipated. Figure 9 plots the evolution of average reflectivity for each cell on a common time axis with an origin when each cell reached its observed average reflectivity peak.

TABLE 3. Characteristics of example drizzle cells (see also Fig. 10). Columns represent assigned cell number, times and dates cells are present in the C-band radar field of view, lifetime area-averaged reflectivity, average advection speed and direction of origin (° from north), bounding box size, and other cell properties.

	Start–end times and date	Avg dBZ	Avg advection speed (m s^{-1}) and direction	Bounding box size (km^2)	Cell properties
1	1245–1350 UTC 18 Oct	8.9	8.3, 125°	13.5 by 9.5	Appear, grow, fade, advect out
2	1325–1440 UTC 18 Oct	8.6	7.9, 118°	11.5 by 10	Advect in, fade
3	0150–0300 UTC 19 Oct	12.6	8.3, 127°	10.5 by 14	Advect in, grow, advect out
4	0210–0300 UTC 19 Oct	9.7	8.3, 127°	10.5 by 22	Advect in, split, fade
5	0220–0320 UTC 19 Oct	6.5	8.3, 127°	12 by 12	Advect in, fade
6	0830–0940 UTC 21 Oct	11.4	9.0, 112°	13.5 by 22	Advect in, grow, split, fade, advect out
7	0905–1030 UTC 21 Oct	12.3	9.0, 112°	7 by 16.5	Advect in, grow, merge with another cell, advect out
8	0945–1100 UTC 21 Oct	12.3	9.0, 112°	10.5 by 18.5	Advect in, grow, advect out

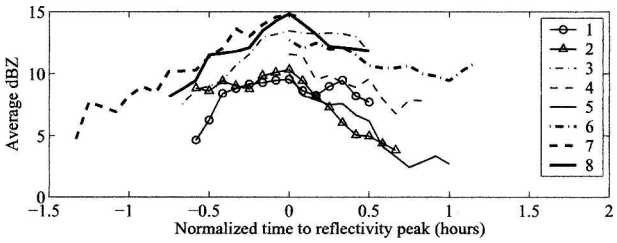

FIG. 9. Average C-band radar reflectivity for eight example cells on 3 days. Time scale is normalized with respect to time at which cells reach their observed peak average reflectivity. Drizzle cell numbers refer to Table 3.

From this figure, we can infer that the typical lifetime of a large drizzle cell is a little over 2 h.

A 2D spatial autocovariance analysis was performed for each example cell at each time step. The *e*-folding distance was determined for each cell by fitting an exponential to a plot of the time mean of each cell's spatial autocovariance of reflectivity. The *e*-folding distance for the analyzed cells is about 2.5 km, showing that the reflectivity peaks in drizzle cells are quite localized.

Small areas with radar reflectivity larger than 20 dBZ (e.g., Fig. 8) were not uncommon during the on-station period. The spatially averaged drizzle cell reflectivity peaks of 9–15 dBZ seen in Fig. 9 imply cloud-base rain rates of 0.5–1.6 mm h^{-1} using reflectivity–rain rate relationships derived by Comstock et al. (2004). The corresponding uncertainty envelope spans 0.3–2.9 mm h^{-1}.

To sustain drizzle cells with drizzle rates of 1 mm h^{-1} over lifetimes of 2 h, cloud condensate must be continuously regenerated by the transfer of moisture from the subcloud layer to the cloud, as found by earlier studies (Paluch and Lenschow 1991; Austin et al. 1995; Pincus et al. 1997; Wood 2004). Otherwise, maximum cell lifetimes would be about 20 min, as estimated using a rainout timescale of $\tau_{\text{rainout}} \simeq \text{LWP}/R$, where LWP (liquid water path) ≈ 300 g m^{-2} and $R \approx 1$ mm h^{-1}.

GOES infrared satellite images are shown in Fig. 10 to provide larger-scale context for the eight example cells. The approximate drizzle cell positions at the start of their radar-observed lifetimes were advected to the IR image times and are marked in each image. The visible image corresponding to the first two cells (Fig. 10a) is provided in Fig. 11a. All of the example drizzle cells occurred in regions of broken clouds.

6. Conceptual model of the Sc boundary layer

From the above observations, we have synthesized conceptual models for coupled and drizzling Sc regimes. Modulation of the Sc boundary layer by the diurnal cycle, described in the introduction, explains the occurrence of drizzle primarily in the early morning. However, both Figs. 3 and 4 indicate that while the majority of the drizzle (approximately 80% of the on-station period hours containing drizzle) occurred between midnight and noon local time, drizzle was not uncommon during other times of the day. In general, drizzle characteristics varied greatly during the EPIC 2001 Sc on-station period. Qualitatively, we found that the drizzle was often associated with patches of open cellular convection embedded within typically closed-cell Sc sheets. Stevens et al. (2005) associated these "pockets of open cells" (POCs) with higher drizzle rates than the closed-cell regions, based on findings from DYCOMS II (see vanZanten et al. 2005) as well as a preliminary analysis of some of the results above.

Indeed, Fig. 10 shows that all of the strongly drizzling

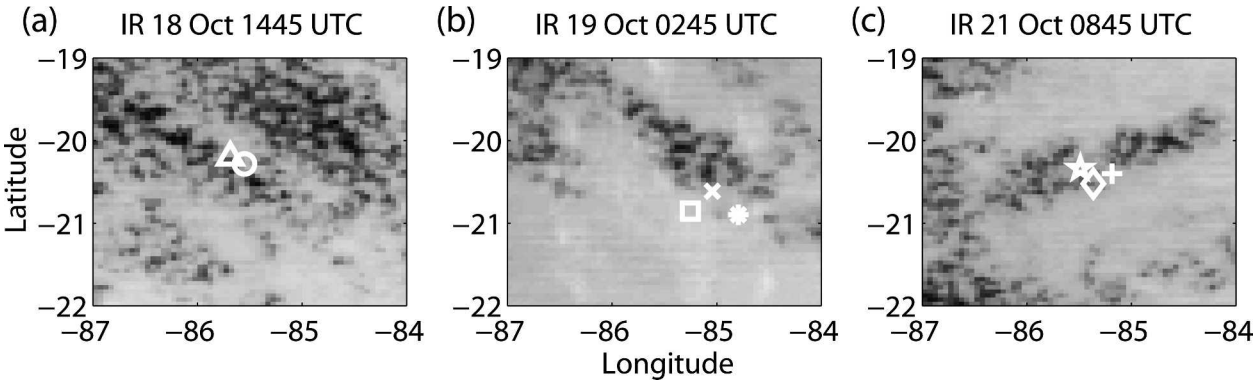

FIG. 10. GOES IR satellite images at (a) 1445 UTC 18 Oct, (b) 0245 UTC 19 Oct, and (c) 0845 UTC 21 Oct. Drizzle cell start positions are shown. Cells 1 (triangle) and 2 (circle) are on 18 Oct (a); cells 3 (asterisk), 4 (square), and 5 (×) are on 19 Oct (b); and cells 6 (plus sign), 7 (diamond), and 8 (star) are on 21 Oct (c), where cell numbers refer to Table 3.

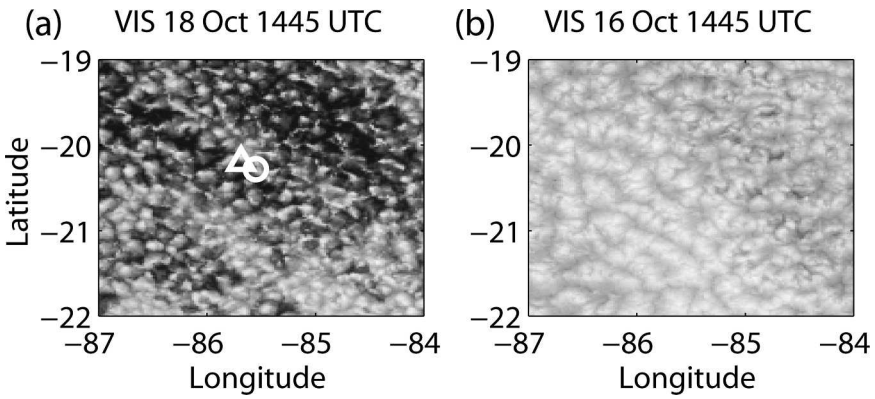

FIG. 11. GOES visible satellite images. (a) Open-cell mesoscale cellular convection at 1445 UTC 18 Oct, and (b) closed cells at 1445 UTC 16 Oct. Drizzle cell start positions are shown (a) for cells 1 (triangle) and 2 (circle), where cell numbers refer to Table 3. The infrared image corresponding to (a) is shown in Fig. 10a.

example cells discussed in the previous section occur in or near POCs. Figures 10a and 11a show a morning (1445 UTC, 0845 local time) example of open cellular convection with drizzle, while Fig. 11b shows a visible image of closed-cell convection in the coupled regime at the same time of the day. The MMCR (Fig. 3) and C-band radar (not shown) indicate that it was not drizzling at the ship at this time.

Figure 3 shows that high drizzle rates (top panel) usually correspond with broken clouds (third and fourth panels). Table 2, which gives standard deviations of cloud and surface properties for each of the boundary layer regimes, also supports the hypothesis that the coupled regime is associated with closed cells and the drizzling regime with open cells. The highest degree of variance for cloud parameters, corresponding to the largest degree of horizontal inhomogeneity in cloud properties, is found in the drizzling regime. The coupled regime shows the least variance and, therefore, the most horizontal homogeneity. Likewise, closed-cell Sc regions (Fig. 11b) have much less mesoscale inhomogeneity than open cells (Fig. 11a). Hence, our results and conceptual models of the coupled and drizzling regimes can also be interpreted as corresponding to closed and open mesoscale cellular structure, respectively. The following subsections detail the conceptual models developed for each regime.

a. Coupled regime

Table 4 shows simultaneous cross correlations between selected pairs of mesoscale bandpass-filtered time series for each of the three regimes. In the coupled (closed cell) regime, correlations indicate that it is warmer and moister below patches of thicker cloud with lower cloud base and higher cloud top. Although the signal becomes less certain when the three regimes are analyzed separately, coherence-squared and phase plots for the coupled time periods (not shown) are similar to Fig. 2, suggesting convergence coincident with warm regions, particularly on scales of close to 20–25 km. These scales are consistent with the inspection of GOES visible imagery (e.g., Fig. 11b), which showed roughly 15–60-km-diameter closed cells during the EPIC 2001 Sc on-station period. Atkinson and Zhang (1996) reviewed numerous field investigations of open and closed cells and also found that closed-cell diameters tend to fall between 24 and 53 km. Figure 12a illustrates a conceptual model of a closed cell that re-

TABLE 4. Cross correlations for bandpass-filtered ship data series in coupled, less-coupled, and drizzling regimes. Statistically significant correlations (99% confidence level) are in boldface. The parameters include virtual temperature T_v, water vapor mixing ratio q, wind speed U, cloud base cb, lifting condensation level LCL, cloud top ctop, cloud thickness cthk, and downwelling longwave radiation LW.

Parameter pairs	T_v, q	T_v, U	T_v, cb	q, cb	q, LCL	cb, ctop	cthk, LW	cthk, T_v	cthk, q
Coupled	**0.30**	0.03	−0.23	**−0.64**	**−0.93**	**−0.41**	**0.57**	**0.43**	**0.64**
Less coupled	**−0.27**	−0.06	**0.32**	−0.22	**−0.85**	0.03	**0.76**	**−0.45**	0.20
Drizzling	**−0.53**	−0.07	**0.38**	−0.19	**−0.87**	0.08	**0.81**	**−0.33**	0.07

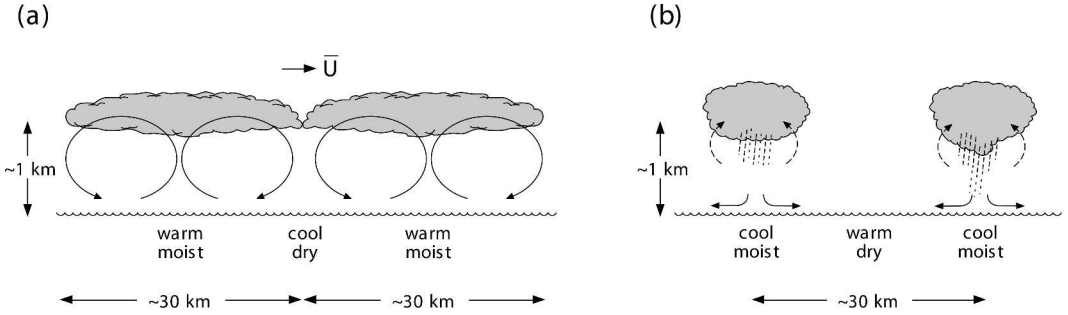

FIG. 12. Conceptual models of the boundary layer circulations in (a) the coupled (closed cell) regime, such as those depicted in Fig. 11b, and (b) the drizzling (open cell) regime, such as those in Fig. 11a. The mean wind, $\overline{U}$, in (a) relates to the underlying circulation, which represents perturbations in U. Here, $\overline{U}$ is not depicted in (b) because for the open-cell case, the circulation has no known directional dependence. The sketch in (b) also represents the variability of the drizzling regime by showing that some of the precipitation reaches the surface, but much of it evaporates in the boundary layer. The sketches are not drawn to scale.

flects these findings. It shows surface convergence and, therefore, updrafts in regions of high moisture and T_v under thicker clouds.

b. Less-coupled regime

During the EPIC 2001 Sc on-station period, the soundings in Fig. 6 suggest that decoupling was incomplete; that is, there was some amount of mixing throughout the boundary layer, hence our diagnosis of the "less coupled" regime. If decoupling had taken place, the surface layer would have rapidly moistened and produced a second cloud layer at its top.

The less-coupled regime was not associated solely with a particular cloud regime (open or closed cells), but was instead linked to afternoon cloud thinning. Table 1 documents the thinner clouds during less-coupled periods. Figure 4 shows that this regime occurred every afternoon but was rare at night (when a less well-mixed boundary layer was generally associated with drizzle). During EPIC 2001 Sc, all of the high-resolution data were obtained in the surface layer, so we do not have sufficient information to lay out a complete conceptual model for the less-coupled boundary layer.

c. Drizzling regime

The drizzling boundary layer is nonuniform, but some vertical mixing must be occurring throughout the boundary layer because moisture is reaching the cloud layer and replenishing it. Otherwise, the drizzle cells would not persist as long as they do (section 5). Paluch and Lenschow (1991) showed evidence that this replenishment was occurring on small eddy scales. It is possible that entrainment of relatively moist air from above the inversion may also play a role in enhancing drizzle in some cases. This was observed in drizzling periods in the northeast Pacific during TEPPS Sc (Yuter et al. 2000) and DYCOMS II (Stevens et al. 2003). However, Fig. 6 shows that only 6 of the 16 drizzling soundings from EPIC have a mixing ratio exceeding 2 g kg^{-1} above the inversion.

Table 4 shows that, in the drizzling regime, T_v is negatively correlated with surface q as well as cloud thickness, while T_v and cloud-base height are positively correlated. Although cooler air also tends to be more moist, surface moisture does not correlate well with cloud base or thickness. This may be partly because temperature has more mesoscale variability than moisture at the surface in the drizzling regime (Table 2). Collectively, the relationships suggest that evaporatively cooled air tends to pool beneath lower cloud bases and thicker clouds.

Figure 12b shows a conceptual model of the drizzling, open-cell boundary layer. Moist updrafts are likely to be found beneath cloud elements, but they may not be evident at the surface or they may distorted by the moist, evaporatively cooled downdrafts. These updrafts also contribute to the replenishment of moisture into the cloud layer. The spatial scales portrayed in Fig. 12b are consistent with EPIC 2001 Sc observations, such as those in Fig. 8, and the visual inspection of GOES visible satellite data (e.g., Fig. 11a) that showed cells roughly 20–60 km in diameter. Atkinson and Zhang (1996) reported that open cells are typically about 30 km across, and Wood and Hartmann (2004) found that the cloudy parts of open cells are typically about 10 km across, while an entire open cell is about 36 km in diameter.

7. Discussion and conclusions

The EPIC 2001 Sc cruise and the WHOI IMET buoy provided comprehensive datasets for studying 10–100-

km mesoscale variability of the stratocumulus-topped boundary layer in the southeast Pacific. Power spectra of all surface parameters show a spectral break in the mesoscales in addition to a strong diurnal peak. The boundary layer structure and mesoscale organization are modulated by the diurnal cycle. During the night the boundary layer is well mixed, and the cloud layer thickens. Early in the morning the cloud is often sufficiently thick to create drizzle. Daily decoupling, which peaks at around 1500 local time, is initiated by morning solar absorption in the Sc clouds, but may be aided by the stabilizing effect of subcloud drizzle evaporation (Caldwell et al. 2005).

To illuminate the potential effects of drizzle on the dynamics of the boundary layer and Sc cloud properties, we subdivided the EPIC dataset into coupled, less-coupled, and drizzling regimes, which were analyzed separately. The coupled boundary layer is the most horizontally homogeneous and vertically well mixed, and corresponds to mainly nocturnal closed cells commonly seen in coastal Sc regions. Warm, moist updrafts underlie thicker cloud patches and cooler, drier air underlies the surrounding rings of thinner cloud. For the most part, this model is consistent with past work based on much sparser data, some of it in different synoptic settings. For example, Moyer and Young (1994) developed a closed-cell model using aircraft observations from FIRE in the northeast Pacific, and Rothermel and Agee (1980) also developed a model based on limited aircraft data from the Air Mass Transformation Experiment in 1975 (AMTEX-75) in a cold-air outbreak in the East China Sea. Consistent with our model for Sc clouds, the latter study found warm, moist, rising air in the center, and drier, sinking air on the edges of closed cells. They also showed a double temperature wave below the closed cell at the surface, but this result has not been found by others (Atkinson and Zhang 1996) and may reflect inadequate sampling.

The less-coupled regime was almost exclusively observed during daytime and was associated with thinner, more broken clouds of lower albedo. Even in this regime, the vertical moisture gradients were modest. It is not possible to determine the mesoscale circulations in the less-coupled boundary layer from surface measurements during EPIC 2001 Sc.

The drizzling regime corresponds to increased mesoscale variability in cloud and boundary layer properties compared to the nonprecipitating regimes, with moist, evaporatively cooled downdrafts beneath the rings of thicker, precipitating cloud. This corroborates the recent suggestions of Stevens et al. (2005) that open-cell cloud patterns correspond to heavy drizzle.

Our findings for the drizzling regime are largely consistent with prior investigations of open-cell structure; for example, Brümmer et al. (1986) found cooler, moist air below cloudy regions and divergence at the surface in the clear regions in North Sea open cells. However, the open cells documented in previous work have been primarily associated with cold-air outbreaks, where they are maintained by different mechanisms, and where they are not necessarily characterized by strong drizzle. Although our models for closed and open cells are similar to those drawn for cold-air outbreaks, the models described here (and in particular the connection of POCs and drizzle) are only intended to apply to the core subtropical Sc regions.

One of the marked characteristics of "traditional" open cells is a strong air–sea temperature difference, driven by the advection of cold air over a warmer sea surface. The temperature difference is typically between 2° and 5°C but can be as much as 10°C (Atkinson and Zhang 1996). There was some evidence for enhanced air–sea temperature differences in the drizzle regime during EPIC 2001 Sc. However, these appear to be caused by cold pools of air formed by the evaporation of drizzle. The mean air–sea temperature difference during the drizzling regime was about $2.2 \pm 0.6°$, 1°C larger than that for the coupled (closed cell) regime (Table 2). It is possible that the increased air–sea temperature difference during the drizzling regime plays some role in maintaining the open-cell structure in Sc clouds.

Distinct drizzle cells in this region, as detected by the shipboard C-band radar, can have contiguous areas with reflectivity greater than 5 dBZ up to about 100 km^2 and cell-averaged reflectivity up to about 15 dBZ (corresponding to about 1 mm h^{-1} rain rate). Because they last for about 2 h instead of raining themselves out within about half an hour, drizzle cells are apparently regaining moisture via updrafts even as they are losing water due to precipitation. Since most of the drizzle evaporates in the boundary layer, drizzle "recycling" may be playing a key role in sustaining the mesoscale cloud variability and drizzle cell longevity.

In this analysis, we did not address the aerosol characteristics of the boundary layer. Increased aerosol concentrations may influence cloud droplet concentrations and the formation of drizzle (e.g., Albrecht 1989). Observations of Sc clouds in the northeast and southeast Pacific by Stevens et al. (2005), Bretherton et al. (2004), and Kollias et al. (2004) suggest that high drizzle rates are associated with low cloud droplet concentrations. However, further intensive observations and modeling work will be required to quantify the importance of aerosols on the characteristics of drizzle and Sc cloud properties.

The apparent effect of drizzle in promoting mesoscale variability and more inhomogeneous cloud cover, even when the drizzle mainly evaporates above the surface, implies a strong connection between drizzle and cloud radiative forcing. This connection will be a challenge to realistically represent in climate models, but may play an important role in modulating the indirect effect of both anthropogenic and natural aerosols on regional scales and on the global climate.

Acknowledgments. The authors wish to acknowledge Beth Tully for graphics support. Robert Weller and his group at WHOI provided buoy data, funded by the NOAA Office of Global Programs, Climate Observation Program. Christopher Fairall, Taneil Uttal, and Duane Hazen of NOAA/ETL provided MMCR data and information. We are also grateful to the crew of the NOAA *RHB* for their assistance in collecting observations during the EPIC cruise and to Bjorn Stevens and Donald Lenschow for their comments and suggestions. This research was funded by NSF Grant ATM-0082384, NASA Grants NAG5S-10624 and NNG04GF33A, and a NDSEG fellowship.

REFERENCES

Agee, E. M., and F. E. Lomax, 1978: Structure of the mixed layer and inversion layer associated with patterns of mesoscale cellular convection during AMTEX 75. *J. Atmos. Sci.,* **35,** 2281–2301.

——, T. S. Chen, and K. E. Dowell, 1973: A review of mesoscale cellular convection. *Bull. Amer. Meteor. Soc.,* **54,** 1004–1012.

Albrecht, B. A., 1989: Aerosols, cloud microphysics, and fractional cloudiness. *Science,* **245,** 1227–1230.

Atkinson, B. W., and J. W. Zhang, 1996: Mesoscale shallow convection in the atmosphere. *Rev. Geophys.,* **34,** 403–431.

Austin, P., Y. Wang, R. Pincus, and V. Kujala, 1995: Precipitation in stratocumulus clouds: Observations and modeling results. *J. Atmos. Sci.,* **52,** 2329–2352.

Bolton, D., 1980: The computation of equivalent potential temperature. *Mon. Wea. Rev.,* **108,** 1046–1053.

Bretherton, C. S., T. Uttal, C. W. Fairall, S. E. Yuter, R. A. Weller, D. Baumgardner, K. Comstock, and R. Wood, 2004: The EPIC 2001 stratocumulus study. *Bull. Amer. Meteor. Soc.,* **85,** 967–977.

Brümmer, B., T. Fischer, and S. Zank, 1986: Aircraft observations of open cellular structures during KonTur. *Contrib. Atmos. Phys.,* **59,** 162–184.

Caldwell, P., C. S. Bretherton, and R. Wood, 2005: Mixed layer budget analysis of the diurnal cycle of entrainment in southeast Pacific stratocumulus. *J. Atmos. Sci.,* **62,** 3775–3791.

Comstock, K., R. Wood, S. E. Yuter, and C. S. Bretherton, 2004: The relationship between reflectivity and rain rate in and below drizzling stratocumulus. *Quart. J. Roy. Meteor. Soc.,* **130,** 2891–2918.

Cox, S. K., D. S. McDougal, D. A. Randall, and R. A. Schiffer, 1987: FIRE—The First ISCCP Regional Experiment. *Bull. Amer. Meteor. Soc.,* **68,** 114–118.

Cronin, M. F., N. Bond, C. Fairall, J. Hare, M. J. McPhaden, and R. A. Weller, 2002: Enhanced oceanic and atmospheric monitoring underway in eastern Pacific. *Eos, Trans. Amer. Geophys. Union,* **83,** 205, 210–211.

Delecluse, P. M. K. D., Y. Kitamura, S. G. H. Philander, M. Suarez, and L. Bengtsson, 1998: Coupled general circulation modeling of the tropical Pacific. *J. Geophys. Res.,* **103,** 14 357–14 374.

Garay, M. J., R. Davies, C. Averill, and J. A. Westphal, 2004: Actinoform clouds: Overlooked examples of cloud self-organization at the mesoscale. *Bull. Amer. Meteor. Soc.,* **85,** 1585–1594.

Hartmann, D. L., M. E. Ockert-Bell, and M. L. Michelson, 1992: The effect of cloud type on Earth's energy balance: Global analysis. *J. Climate,* **5,** 1281–1304.

Klein, S. A., and D. L. Hartmann, 1993: The seasonal cycle of low stratiform clouds. *J. Climate,* **6,** 1587–1606.

Kollias, P., C. W. Fairall, P. Zuidema, J. Tomlinson, and G. A. Wick, 2004: Observations of marine stratocumulus in SE Pacific during the PACS 2003 cruise. *Geophys. Res. Lett.,* **31,** L22110, doi:10.1029/2004GL020751.

Kraus, E. B., 1963: The diurnal precipitation change over the sea. *J. Atmos. Sci.,* **20,** 551–556.

Menzel, W. P., and J. F. W. Purdom, 1994: Introducing GOES-I: The first in a new generation of geostationary operational satellites. *Bull. Amer. Meteor. Soc.,* **75,** 757–780.

Moran, K. P., B. E. Martner, M. J. Post, R. A. Kropfli, D. C. Welsh, and K. B. Widener, 1998: An unattended cloud-profiling radar for use in climate research. *Bull. Amer. Meteor. Soc.,* **79,** 443–455.

Moyer, K. A., and G. S. Young, 1994: Observations of mesoscale cellular convection from the marine stratocumulus phase of FIRE. *Bound.-Layer Meteor.,* **71,** 109–133.

Nastrom, G. D., and K. S. Gage, 1985: A climatology of atmospheric wavenumber spectra of wind and temperature observed by commercial aircraft. *J. Atmos. Sci.,* **42,** 950–960.

Nicholls, S., and J. Turton, 1986: An observational study of the structure of stratiform cloud sheets: Part II. Entrainment. *Quart. J. Roy. Meteor. Soc.,* **112,** 461–480.

Orlanski, I., 1975: A rational subdivision of scales for atmospheric processes. *Bull. Amer. Meteor. Soc.,* **56,** 527–530.

Paluch, I. R., and D. H. Lenschow, 1991: Stratiform cloud formation in the marine boundary layer. *J. Atmos. Sci.,* **48,** 2141–2158.

Pincus, R., M. Baker, and C. S. Bretherton, 1997: What controls stratocumulus radiative properties? Lagrangian observations of cloud evolution. *J. Atmos. Sci.,* **54,** 2215–2236.

Rossow, W. B., C. Delo, and B. Cairns, 2002: Implications of the observed mesoscale variations of clouds for the earth's radiation budget. *J. Climate,* **15,** 557–585.

Rothermel, J., and E. M. Agee, 1980: Aircraft investigation of mesoscale cellular convection during AMTEX 75. *J. Atmos. Sci.,* **37,** 1027–1040.

Ryan, M., M. J. Post, B. Martner, J. Novak, and L. Davis, 2002: The NOAA Ron Brown's shipboard Doppler precipitation radar. Preprints, *Sixth Symp. on Integrated Observing Systems,* Orlando, FL, Amer. Meteor. Soc., 46–48.

Stevens, B., W. R. Cotton, G. Feingold, and C.-H. Moeng, 1998: Large-eddy simulations of strongly precipitating, shallow, stratocumulus-topped boundary layers. *J. Atmos. Sci.,* **55,** 3616–3638.

——, and Coauthors, 2003: Dynamics and Chemistry of Marine Stratocumulus—DYCOMS II. *Bull. Amer. Meteor. Soc.,* **84,** 579–593.

——, G. Vali, K. Comstock, R. Wood, M. C. vanZanten, P. H. Austin, C. S. Bretherton, and D. H. Lenschow, 2005: Pockets of open cells (POCs) and drizzle in marine stratocumulus. *Bull. Amer. Meteor. Soc.,* **86,** 51–57.

vanZanten, M., B. Stevens, G. Vali, and D. Lenschow, 2005: Observations of drizzle in nocturnal marine stratocumulus. *J. Atmos. Sci.,* **62,** 88–106.

von Storch, H., and F. W. Zwiers, 1999: *Statistical Analysis in Climate Research.* Cambridge University Press, 484 pp.

Welch, P., 1967: The use of fast Fourier transform for the estimation of power spectra: A method based on time averaging over short, modified periodograms. *IEEE Trans. Audio Electroacoust.,* **AU-15,** 70–73.

Wood, R., 2005: Drizzle in stratiform boundary layer clouds. Part I: Vertical and horizontal structure. *J. Atmos. Sci.,* **62,** 3011–3033.

Yuter, S. E., Y. L. Serra, and R. A. Houze, 2000: The 1997 Pan American Climate Studies Tropical Eastern Pacific Process Study. Part II: Stratocumulus region. *Bull. Amer. Meteor. Soc.,* **81,** 483–490.